

RSC Advances



This is an *Accepted Manuscript*, which has been through the Royal Society of Chemistry peer review process and has been accepted for publication.

Accepted Manuscripts are published online shortly after acceptance, before technical editing, formatting and proof reading. Using this free service, authors can make their results available to the community, in citable form, before we publish the edited article. This *Accepted Manuscript* will be replaced by the edited, formatted and paginated article as soon as this is available.

You can find more information about *Accepted Manuscripts* in the [Information for Authors](#).

Please note that technical editing may introduce minor changes to the text and/or graphics, which may alter content. The journal's standard [Terms & Conditions](#) and the [Ethical guidelines](#) still apply. In no event shall the Royal Society of Chemistry be held responsible for any errors or omissions in this *Accepted Manuscript* or any consequences arising from the use of any information it contains.

ARTICLE

Polyoxometalate-based layered nano-tubular arrays: Facile fabrication and superior performance for catalysis

Cite this: DOI: 10.1039/x0xx00000x
Hongpeng Zhen,^{a,b} Xiaolin Li,^b Lijuan Zhang,^{*a} Huan Lei,^a Chao Yu,^a Yunshan Zhou,^{*b} Sadaf ul Hassan,^a Libo Qin^a and Hafiz Muhammad Asif^a

Received 00th January 2012,
Accepted 00th January 2012

DOI: 10.1039/x0xx00000x

www.rsc.org/

The Keggin type polyoxoanion $PW_{12}O_{40}^{3-}$ -containing one-dimensional nano-tubular arrays with the structure of polyethylenimine/polystyrenesulfonate/poly(allylammonium)/polystyrenesulfonate)₃(poly(allylammonium)/ $PW_{12}O_{40}^{3-}$)₈ were fabricated as a prototype using the layer-by-layer deposition technique in porous anodic aluminum oxide and polycarbonate templates of pore diameter 200 nm, respectively, and characterized by IR, UV-vis and SEM. The resulted nano-tubes have uniform diameter of 180 ± 20 nm and uniform wall thickness of 30 ± 5 nm. These arrays have showed superior performance in UV light irradiated photo-degradation of Rhodamine B selected as a representative under mild conditions in view of both catalytic efficiency and operating convenience due to the confinement both in the latitudinal and radial direction within the nano-tubes. Remarkably, catalytic activity of the nano-tubular arrays could be recovered by means of simple immersion in the polyoxoanion solution when catalytic reactivity was faded, which is vital in view of practical application. The total organic carbon changes and GC-MS measurements were conducted to identify the degradation products, and the hydroxyl radicals mechanism was found to be adopted by the photo-degradation reaction.

Introduction

Polyoxometalates (POMs) are a class of discrete transition metal anionic clusters with abundant compositions, structures and versatile properties leading to their successful applications in various fields.¹⁻³ Among the important/potential applications, the catalytic activities of POMs are the most fascinating feature and their outstanding aspects are homo-/heterogeneous acid or redox catalyses⁴⁻⁸ with the advantages such as photo-/thermal stability,^{9,10} non-toxicity,¹¹ low cost and environment friendly behavior.¹² However, most POMs are highly-soluble in aqueous solution to form a homogeneous catalyst which is often inconvenient for industrial purposes.^{13,14} In contrast, heterogeneous catalysis is easier to run and separate, yielding a sustainable catalytic process, and many efforts have been manipulated for heterogenization of homogeneous POMs-based catalysts such as the syntheses of heterogeneous catalysts by combining POMs with counter cations such as K^+ , CS^+ , NH_4^+ ,¹⁵⁻¹⁷ or formation of nanoparticles or/and preparation of the films by coating POMs onto inorganic/organic composition such as TiO_2 , SiO_2 , activated carbon or organic polymer.¹⁸⁻²¹ However, exploring new approaches that can separate POMs catalysts more conveniently from reaction systems with more convenient

recycle process as well as enhanced superior catalytic performance still remains challenging.

Inspired by the continuing great success of nanotubular materials in various fields,^{22,23} incorporating polyoxometalates into nano-tubular arrays may be expected to overcome the limitation i.e., small surface area,²⁴ difficulty in recycle and reuse due to water solubility¹³ as well as to realize upgraded catalytic activity, because of the specific characters such as the nanotubular shape with controllable wall thickness and aperture, high specific surface area exhibiting more active sites, the confinement both in the latitudinal and radial direction within the nano-tubes and possible synergistic and coupling effects of arrays. In this work, we report the fabrication and characterization of nano-tubular arrays based on the well-known α -Keggin type $H_3PW_{12}O_{40}$, which is selected as representative due to its superior performance as catalyst^{15,25-33} (1882 references is found containing the concept "tungstophosphoric acid catalysis" in SciFinder database on Jan 16, 2015). The nano-tubular arrays showed excellent performance as a photo-catalyst to degrade RhB (difficult to degrade completely by conventional methods and also suspected to be carcinogenic) under UV-vis. light irradiation. Importantly, the catalytic activity of the POMs nano-tubular

arrays can be renewed by simple immersion in a $\text{H}_3\text{PW}_{12}\text{O}_{40}^-$ containing solution when catalytic reactivity is faded after recycling for many times, which is very important in view of practical application.

Experimental

Polyethylenimine (PEI, MW 50000) and sodium polystyrenesulfonate (PSS, MW 70000) were purchased from Aldrich. Poly(allylammonium chloride) (PAH, MW 70000) was purchased from Alfa Aesar. The solution of PEI (10 mg/mL), PSS (2 mg/mL) and PAH (1 mg/mL) each containing 0.1 mol/L of NaCl to enhance ionic strength, was prepared with pH 1.5 adjusted by dilute HCl, respectively. $\text{H}_3\text{PW}_{12}\text{O}_{40}\cdot\text{nH}_2\text{O}$ and RhB were purchased from Sinopharm Chemical Reagent Beijing Co., Ltd. All reagents used in this work were of analytical grade and used as received. Deionized water was used throughout the experiments. Porous anodic aluminium oxide membrane (AAO template: diameter 25mm, pore diameter 200nm, average film thickness 60 μm) and Nucleporetrack-etched polycarbonate membranes (PC template: diameter 25 mm, pore diameter 200 nm, average film thickness 20 μm) were purchased from Whatman corp. The structures of the reactants used are shown in Fig. 1.

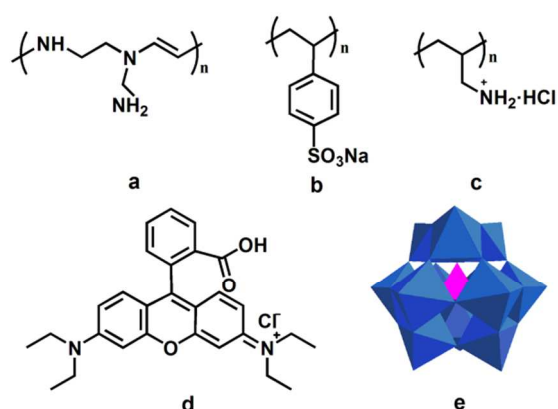


Fig. 1. Structures of the polyelectrolyte PEI (a), PSS (b), PAH (c), dye RhB (d), and the anion $\text{PW}_{12}\text{O}_{40}^{3-}$ (e).

Instruments and techniques of measurement

The FT-IR spectra were recorded on a MAGNA-IR 750 (Nicolet) spectrophotometer with KBr pellet in the range of 400–4000 cm^{-1} . Light intensity was recorded by radiometer FZ-A (the photoelectric instrument factory of Beijing Normal University, China). Scanning electron microscopy (SEM) and energy dispersive X-ray spectroscopy were obtained on a Zeiss Supra 55 scanning electron microscopy. The UV-vis. spectra were recorded on a SHIMADZU UV-2550 spectrometer. The photo-reaction was conducted under a 250 W high-pressure mercury lamp with a light intensity of 22 mW/cm^2 . GC/MS analyses were carried out on a Shimadzu GC/MS QP2010 system equipped with a DB-5 MS capillary column (30 mm \times 0.25 mm). The temperature program of the column was set as follows: at 60 $^{\circ}\text{C}$, hold time = 1 min; from 60 to 250 $^{\circ}\text{C}$, rate 20 $^{\circ}\text{C}/\text{min}$. TOC measurement was performed on a Shimadzu

TOC-5000A analyser. Photoluminescence spectra were obtained on a Hitachi F-7000 fluorescence spectrophotometer with emission slit of 5 nm using 150W xenon lamp as the light source. The millipore filter setup for preparing nano-tubular array and carrying out photo-catalysis reaction was purchased from Auto science Co., Ltd (40 ml in volume and 25 mm in diameter) (Fig. S1).

Preparation of $\text{PEI/PSS}/(\text{PAH/PSS})_3(\text{PAH/PW}_{12}\text{O}_{40}^{3-})_8$ nano-tubular arrays within porous templates

The AAO template was kept on the millipore filter (Fig. S1), and pressure was adjusted to 0.020 MPa by a buffering device to prevent it from breaking. Firstly, 20 ml deionized water was flowed through the template from each side under low pressure condition, then 20 mL PEI solution was flowed through the template from each side. Subsequently, the template was immersed into deionized water for 10 min and then washed with 10 mL deionized water. Similarly, PSS and PAH were alternately adsorbed onto the inner wall of porous template forming a precursor film with the structure of $(\text{PEI/PSS})/(\text{PAH/PSS})_3$. Then, PAH and $\text{PW}_{12}\text{O}_{40}^{3-}$ were alternately adsorbed onto the precursor film from PAH and $\text{H}_3\text{PW}_{12}\text{O}_{40}$ solution (10^{-3} mol/L), respectively, resulting in the formation of layered nano-tubular arrays with a structure of $\text{PEI/PSS}/(\text{PAH/PSS})_3(\text{PAH/PW}_{12}\text{O}_{40}^{3-})_8$ within the pores of AAO template (denoted $\text{PW}_{12}\text{-AAO}$). All the preparation processes were performed under ambient conditions. The same procedure was performed when PC template was used, resulting in the formation of nano-tubular arrays with a structure of $\text{PEI/PSS}/(\text{PAH/PSS})_3(\text{PAH/PW}_{12}\text{O}_{40}^{3-})_8$ within the pore of PC template (denoted $\text{PW}_{12}\text{-PC}$). The fabrication process of POM/polyelectrolyte nano-tubular arrays through LBL coating and sequentially release of nano-tubes are shown in Fig. 2. Release and collection of nano-tubes from PC template for characterization was carried out by dissolving PC template into chloroform followed by centrifugation of the solution. The method used for release and collection of nano-tubes from AAO template is given in the supporting information.

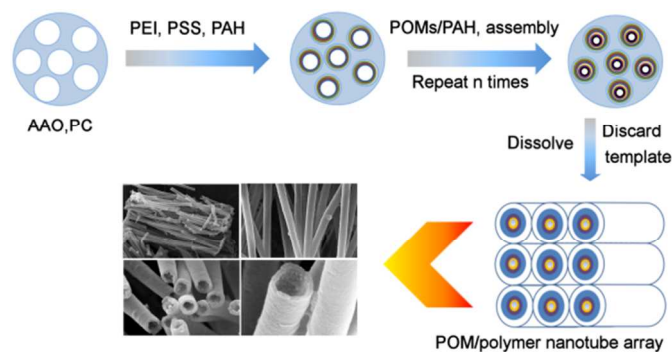


Fig. 2. Schematic diagram illustrating the fabrication process of $\text{PEI/PSS}/(\text{PAH/PSS})_3(\text{PAH/PW}_{12})_8$ nano-tubular arrays within PC/AAO template through LBL coating method and release of the nano-tubes from template for characterization.

Preparation of $\text{PEI/PSS}/(\text{PAH/PSS})_3(\text{PAH/PW}_{12}\text{O}_{40}^{3-})_n$ multi-layered nanofilms on a substrate

A quartz plate was immersed into a fresh piranha solution (conc. $\text{H}_2\text{SO}_4/30\%\text{H}_2\text{O}_2 = 7:3$ (V/V)) at 80°C for 1 h, then rinsed with copious amount of deionized water and dried in a nitrogen atmosphere. After immersion in PEI and PSS, then alternately in PAH and PSS for three cycles and finally alternately in PAH and $\text{H}_3\text{PW}_{12}\text{O}_{40}$ (10^{-3} mol/L) each for 20 min, the coated quartz was characterized by UV-vis in order to monitor and determine the growth of $(\text{PAH}/\text{PW}_{12}\text{O}_{40}^{3-})_n$ bilayers.

Photo-degradation of RhB by $\text{PEI}/\text{PSS}/(\text{PAH}/\text{PSS})_3(\text{PAH}/\text{PW}_{12}\text{O}_{40}^{3-})_8$ nano-tubular arrays

For the photo-catalytic reaction, a high-pressure mercury lamp was used as light source. 40 ml of RhB solution (2 mg RhB per liter of solution) was filtered through the PW_{12} -AAO and PW_{12} -PC catalyst, respectively, which were placed on the millipore filter (Fig S1). All the degradation process was carried out under ambient conditions. The characteristic absorbance changes at $\lambda_{\text{max}} = 554$ nm of RhB were monitored and decoloration efficiency (DE) was calculated by the equation: $\text{DE} = [(A_0 - A_t)/A_0] \times 100\%$, where A_0 stands for the absorbance before reaction, and A_t stands for the absorbance at a given filtration times.

Results and discussion

Fabrication and Characterization of $\text{PEI}/\text{PSS}/(\text{PAH}/\text{PSS})_3(\text{PAH}/\text{PW}_{12}\text{O}_{40}^{3-})_8$ nano-tubular arrays

Despite the so-called layer-by-layer (LBL) technique (viz., immersing a porous template such as AAO and PC alternately into different reactant-containing solution) has been commonly adopted for preparing polyelectrolyte-involving nano-tubes, this method usually suffers from an unavoidable drawback, viz., the entrance of nano-/micro-sized pores of the template are easily blocked due to the strong interaction between the charged polyelectrolyte and the oppositely charged template surface, which prevents the polyelectrolyte molecules and other reactants from entering the pores and anchoring to the inner template walls.³⁴ Consequently, the desired nano-/microtubes cannot be formed inside the pores of the template in the process of alternate immersion.

In our present work, the blockage problem has been well solved by using reduced pressure filtration process, where the pressurized flow of solutions of alternately charged polyelectrolytes/polyoxoanions and neutral washing steps between results in the LbL deposition of a $\text{PEI}/\text{PSS}/(\text{PAH}/\text{PSS})_3(\text{PAH}/\text{PW}_{12}\text{O}_{40}^{3-})_8$ multilayer on the inner walls of the template.

UV-vis. spectrum measurement is an effective method to monitor the growth of film which is formed by LBL technique. Since it is very difficult to directly monitor the growth of each bilayer of $(\text{PAH}/\text{PW}_{12}\text{O}_{40}^{3-})_n$ in the nanopores of template, the growth of POMs film $(\text{PAH}/\text{PW}_{12}\text{O}_{40}^{3-})_n$ on a quartz plate was instead monitored.³⁵ It was found that while the characteristic absorption³⁵⁻³⁶ of the Keggin type PW_{12} appearing at 266 nm attributed to the $\text{W} \leftarrow \text{O}_{\text{b,c}}$ charge transition does not change in position during the whole deposition process, while the absorbance intensity increases linearly with the increasing number of bilayers, $(\text{PAH}/\text{PW}_{12}\text{O}_{40}^{3-})_n$ ($n = 1 \sim 8$) (Fig. 3), which not only confirms that the alternate deposition of negatively charged $\text{PW}_{12}\text{O}_{40}^{3-}$ anions and the positively charged

PAH but also demonstrates that the thickness of the films is precisely controllable. Though this result is obtained from a flat surface and may not be directly extended to a cylindrical type substrate, however, we expect that the same linear relationship exists for growth of $(\text{PAH}/\text{PW}_{12}\text{O}_{40}^{3-})_n$ nano-tubes.

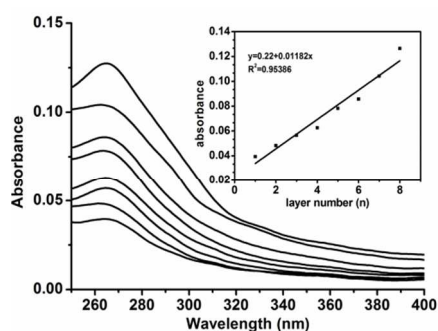


Fig. 3. The UV-vis. spectra of $\text{PEI}/\text{PSS}/(\text{PAH}/\text{PSS})_3(\text{PAH}/\text{PW}_{12}\text{O}_{40}^{3-})_n$ ($n = 1 \sim 8$) multilayered films. The inset shows the linear relationship between absorbance intensity at 266 nm and the number of $(\text{PAH}/\text{PW}_{12}\text{O}_{40}^{3-})$ bilayers, respectively.

The SEM images of $\text{PEI}/\text{PSS}/(\text{PAH}/\text{PSS})_3(\text{PAH}/\text{PW}_{12}\text{O}_{40}^{3-})_8$ nano-tubes released from PC template (Fig. 4) show that the tubes have uniform diameter of 180 ± 20 nm and uniform wall thickness which reaches 30 ± 5 nm. The average thickness of each $(\text{PAH}/\text{PW}_{12}\text{O}_{40}^{3-})$ bilayer is roughly calculated to be ca. 2 nm (Fig. 4b). The SEM images of nano-tubes released from AAO template (Fig. S2) illustrates tubular structures with uniform diameter of $180 \text{ nm} \pm 20 \text{ nm}$, that is closed to the aperture of AAO film with wall thickness of $20 \pm 5 \text{ nm}$ which is a little thinner than nano-tubes released from PC template because of partial dissolution during release process in phosphoric acid (supporting information).

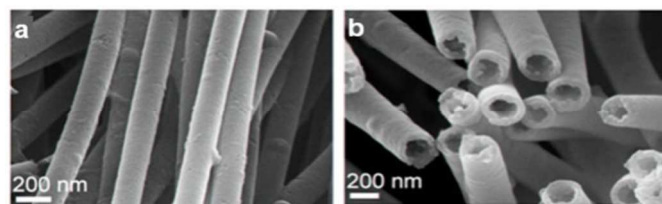


Fig. 4. The SEM images of $\text{PEI}/\text{PSS}/(\text{PAH}/\text{PSS})_3(\text{PAH}/\text{PW}_{12}\text{O}_{40}^{3-})_8$ nano-tubes released from the template of PC: (a) the side view of nano-tubes; (b) the cross-section view of nano-tubes.

FT-IR spectra of $\text{PEI}/\text{PSS}/(\text{PAH}/\text{PSS})_3(\text{PAH}/\text{PW}_{12}\text{O}_{40}^{3-})_8$ nano-tubes (Fig. S3) show the four characteristic peaks^{15,16,35,36} of α -Keggin-type $\text{PW}_{12}\text{O}_{40}^{3-}$: P-O bond in PO_4 ($\nu_{\text{as}} = 1083 \text{ cm}^{-1}$), W-O_b-W bond ($\nu_{\text{as}} = 890 \text{ cm}^{-1}$), W-O_c-W bond ($\nu_{\text{as}} = 800 \text{ cm}^{-1}$) (O_b was the oxygen atom between the two different W_3O_{13} groups, O_c was the oxygen atom in the same W_3O_{13} group) and W=O_d bonds ($\nu_{\text{as}} = 952 \text{ cm}^{-1}$). The red/blue shift of peaks compared to the parent $\text{PW}_{12}\text{O}_{40}^{3-}$ can be attributed to strong attraction between negatively charged $\text{PW}_{12}\text{O}_{40}^{3-}$ and positively charged PAH. The semi-quantitative EDX analyses (Fig. S4) show that the P/W atom ratio of the nano-tubes released from the templates is 1.13:10.52, which is relatively close to the ratio of $\text{PW}_{12}\text{O}_{40}^{3-}$ (P/W = 1:12). The above analyses further confirm that the $\text{PW}_{12}\text{O}_{40}^{3-}$ structure remains intact in the tubular arrays.

Photo-degradation of RhB solution by PEI/PSS/(PAH/PSS)₃(PAH/PW₁₂O₄₀³⁻)₈ nano-tubular arrays

In the preliminary experiments, a PW₁₂-AAO was first immersed into the dye solution for 0.5 h to ensure absorption-desorption equilibrium between the dye and catalyst under dark condition in order to avoid the effect of adsorption of the dye before all the measurement.²⁸ Initially, the influence of light source on the degradation efficiency was discussed. Four types of experiments were taken, 1) under daylight irradiation with bare AAO, 2) under UV light irradiation with bare AAO, 3) under daylight irradiation with the PW₁₂-AAO and 4) under UV light irradiation with the PW₁₂-AAO. Under each of the four conditions, 40 mL of RhB solution was filtered 5 times circularly through a bare AAO and a PW₁₂-AAO, respectively. Results showed that RhB was more remarkably degraded (Fig. 5, Table S1) under UV irradiation in the presence of the nano-tubular arrays as compared to other conditions (Fig. S5). The decoloration efficiency reached a maximum of 94.5% after filtration 5 circular times under UV light irradiation with the PW₁₂-AAO at pH 5. The results indicated that UV irradiation and the nano-tubular arrays catalyst are compulsory for the degradation of RhB.

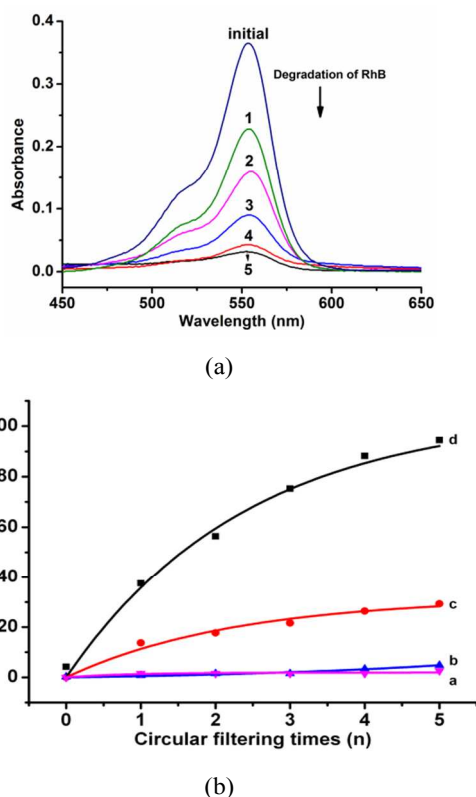


Fig. 5. UV-vis. absorption spectral changes of RhB vs circular filtering times at pH 5 under UV light with PW₁₂-AAO (where the repeating filtration process of filtered RhB solution through the catalyst is called circular filtering). Arrow mark shows the degradation of the RhB with increasing numbers of circular filtering (initial, original RhB solution; 1, first time filtering; 2, second time filtering; 3, third time filtering; 4, fourth time filtering; and 5, fifth time filtering) (a) and the degradation effect of RhB under four different conditions: daylight with bare AAO (line a), UV light with bare AAO (line b), daylight with PW₁₂-AAO (line c) and UV light with PW₁₂-AAO (line d) (b).

Table 1. The effect of pH values on RhB degradation under UV light irradiation with PW₁₂-AAO.

Group	pH	Circulation times	Degradation efficiency (%)
1	6.0	5	79.6
2	5.0	5	94.5
3	4.0	5	95.0
4	3.0	5	97.8

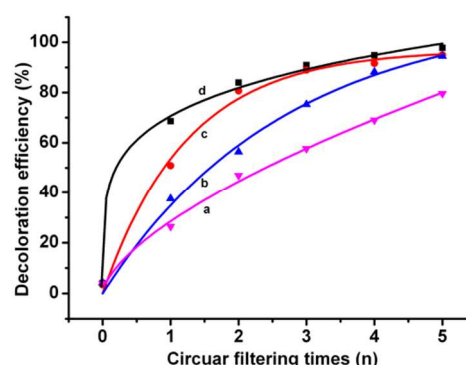


Fig. 6. Effect of pH on photo-degradation of RhB (line a, pH 6.0; line b, pH 5.0; line c, pH 4.0 and line d, pH 3.0) vs. circular filtering times for RhB solution with PW₁₂-AAO under UV light.

As shown in Fig. 6 and Fig. S6, the photo-degradation efficiency varies at different pH values of RhB solution (pH = 3.0, 4.0, 5.0, and 6.0) under the optimal condition, viz., UV light irradiation with PW₁₂-AAO (Table 1). The results show that PEI/PSS/(PAH/PSS)₃(PAH/PW₁₂O₄₀³⁻)₈ nano-tubular arrays have a higher photo-catalytic activity at lower pH value of the reaction system (decoloration efficiency rises from 79.6% (pH = 6.0) to 97.8% (pH = 3.0)), which suggests that the acidic condition is favorable to the degradation of RB molecules in the presence of the catalyst. It should be noted that the observation about pH effect on photocatalytic RhB degradation is analogue to the reported³¹. However, when pH value decreases below 2.5, the acid-base equilibrium of RhB in solution, H₂RhB²⁺ ↔ HRhB⁺ ↔ RhB, will change and RhB may combine more protons to form protonated structure H₂RhB²⁺, which causes blue shift³⁷ of the peak from 554 nm for RhB to 495 nm for H₂RhB²⁺ and consequently it gets difficult to monitor the catalytic efficiency at 554 nm by UV-vis spectral measurement. Therefore, conditions at pH < 2.5 are not considered in this study.

The above results clearly demonstrate that the new nano-tubular arrays system shows high-efficient catalytic ability under the optimal conditions, viz, UV light irradiation and pH = 3. In addition, since AAO template has better parallel array morphology, larger pore density and greater thickness (Fig. S2c, S2d) than PC template (Fig. S7a), total number of nano-tubes and catalyst loading capacity within AAO template is subsequently larger than that within PC template, and the nano-tubular arrays obtained from AAO are better than those from PC in terms of both quantity and regularity. Consequently, much better photo-catalytic decoloration results were obtained when PW₁₂-AAO was used (decoloration efficiency DE = 98%) (Fig. 7, Fig. S8) as compared with PW₁₂-PC (decoloration efficiency DE = 91%) under the same optimal condition.

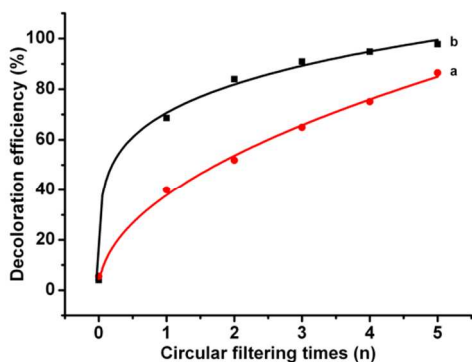


Fig. 7. The comparison of RhB decoloration efficiency with $\text{PW}_{12}\text{-PC}$ (line a) and with $\text{PW}_{12}\text{-AAO}$ (line b) after 5 circular filtering times under the optimal condition.

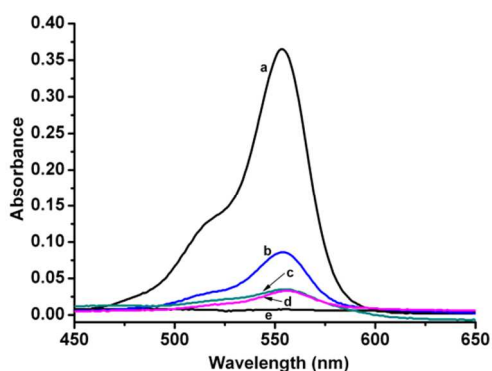


Fig. 8. UV-vis. absorption spectral changes of RhB by filtering once through 5 overlapped $\text{PW}_{12}\text{-PCs}$ (line b) and 5 overlapped $\text{PW}_{12}\text{-AAOs}$ (line c), and filtering 5 circular times through one $\text{PW}_{12}\text{-AAO}$ (line e) and one $\text{PW}_{12}\text{-PC}$ (line d) at the optimal catalytic condition, respectively. Line a is the UV-vis spectrum of original RhB solution.

Interestingly, it was observed that when 5 $\text{PW}_{12}\text{-AAOs}$ and 5 $\text{PW}_{12}\text{-PCs}$ were overlapped respectively and used for once at the optimal catalytic condition, the photo-catalytic decoloration efficiency (DE = 91 % for 5 $\text{PW}_{12}\text{-AAOs}$, 77 % for 5 $\text{PW}_{12}\text{-PCs}$) was a little bit weaker than that for filtering 5 times using a single $\text{PW}_{12}\text{-AAO}$ (DE = 98 %) and a single $\text{PW}_{12}\text{-PC}$ (DE = 90 %) (Fig. 8), respectively. This result could be tentatively attributed to the fact that the middle nanotubular arrays cannot be well irradiated by UV light when five $\text{PW}_{12}\text{-AAOs}$ / $\text{PW}_{12}\text{-PCs}$ overlap tightly together. Despite of this moderate decrease in photo-degradation efficiency, remarkable convenience is appreciated when 5 overlapped $\text{PW}_{12}\text{-AAOs}$ and 5 overlapped $\text{PW}_{12}\text{-PCs}$ were used for once filtering than filtering 5 times using single $\text{PW}_{12}\text{-AAO}$ and single $\text{PW}_{12}\text{-PC}$.

Total organic carbon (TOC) measurement in the degradation of RhB and identification of the final products

Fig. 9 shows the TOC changes during photo-degradation of RhB with circularly filtering times with a $\text{PW}_{12}\text{-AAO}$ under the optimal condition. Prior to degradation, the $\text{PW}_{12}\text{-AAO}$ was immersed into the dye solution (40 ml, 2 mg/L) for 0.5 h in the dark. The maximum TOC removal of RhB was observed to be 42.6 % (from 1.77 to 1.02 ppm) at the point when the solution was almost decolorized after 5 circular filtering times. Therefore, it can be concluded that around half of the dye was

This journal is © The Royal Society of Chemistry 2012

mineralized into CO_2 during the degradation process. However, CO_2 was not the only product as some other organic products were also generated. Under the same conditions, the maximum TOC removal of RhB was 37.7 % with a $\text{PW}_{12}\text{-PC}$ as photocatalyst, which is a little inferior to a $\text{PW}_{12}\text{-AAO}$.

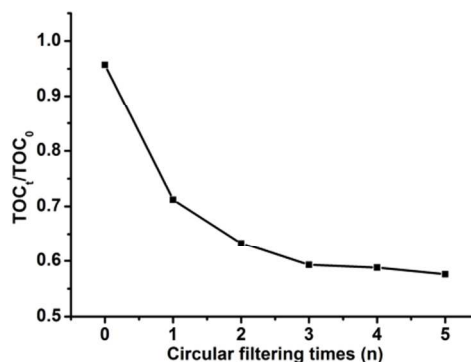


Fig. 9. TOC changes during photo-degradation of RhB versus circularly filtering times with a $\text{PW}_{12}\text{-AAO}$ as catalyst under the optimal condition.

GC/MS technique was used to analyse the final products of RhB degradation. The listed products in Table 2 are the main parts of RhB frameworks besides CO_2 while the other products with very less intensities are neglected. From the above results, it can be concluded that the conjugated xanthene structure of RhB was partially split up during the degradation reaction^{25,26,28,29,31,37,38} in the presence of $\text{PEI/PSS}/(\text{PAH/PSS})_3(\text{PAH/PW}_{12})_8$ nano-tubular arrays under the UV light. The content of each degradation products was calculated according to the TOC changes (Table 2).

Table 2. Final major products of photo-degradation of RhB and their respective amounts detected by GC/MS.

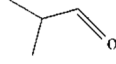
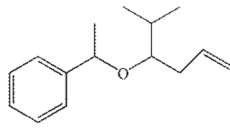
Retention time (min)	Detected product	Relative amount
1.0		0.18
1.25		0.06
5.2	$\text{CH}_3(\text{CH}_2)_6\text{COOH}$	1.00

Photo-catalysis mechanism study

Photo-degradation of RhB has been performed by $\text{PW}_{12}\text{O}_{40}^{3-}$ under various conditions, e.g., sunlight with H_2O_2 ,^{15,25,26} sunlight²⁷⁻³⁰ and UV light.^{31,33} Generally, it is accepted that under UV irradiation, the excited POM molecule induces an electron transition from the highest occupied molecular orbital (HOMO) to the lowest unoccupied molecular orbital (LUMO).

The excited state of POM (POM*) can generate •OH radicals in a water solution, which are extremely powerful oxidizing agent to oxidize organic substrates. While the reduced POM (POM-) produced from the POM* by abstracting an electron from substrates, the electron can be delivered to electron acceptors such as O₂, metal ions and re-change to oxidized POM.^{33,39} Nevertheless, whether photo-catalytic processes in our work adopt similar hydroxyl radicals mechanism needs to be confirmed. It is known that hydroxyl radicals can be detected

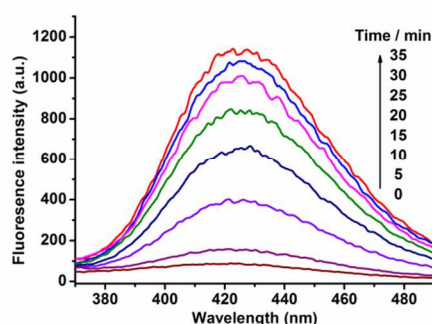


Fig.10. Photoluminescence spectral changes ($\lambda_{\text{max}} = 425$ nm) versus UV light irradiation time on the released nano-tubes from PC templates in a 5×10^{-4} M basic solution of terephthalic acid (excitation light $\lambda = 315$ nm, Voltage = 500V, EX-Slit = 10 nm, EM-Slit = 10 nm).

by the photoluminescence (PL) technique using terephthalic acid (TA) as a probe molecule since the hydroxyl radicals can readily react with TA to produce highly fluorescent product 2-hydroxyterephthalic acid.³³ This method is based on the PL signal of 2-hydroxyterephthalic acid at 425 nm. Moreover, the PL intensity of 2-hydroxyterephthalic acid is proportional to the concentration of •OH radicals which are produced from POMs catalysis. So, a similar procedure for the measurement of photo-catalytic activity is carried out whereby just the RhB aqueous solution is replaced by the 5×10^{-4} M TA aqueous solution (TA was dissolved in 2×10^{-3} M NaOH solution). A gradual increase in PL intensity at about 425 nm (excited by 315 nm UV-light) is observed with an increasing irradiation time for the nano-tubes released from PC templates (Fig.10), while no PL increase is observed in the absence of UV light or the nano-tubes. This suggests that the fluorescence is due to the chemical reactions between terephthalic acid and •OH produced at the catalyst/water interface under UV illumination.³³ Further observation indicates that the PL intensity change is not linear with the irradiation time. This can be ascribed to the fact that PW₁₂ catalyst is not stable in such high basic condition and can be decomposed gradually.

Thus, although it is difficult to demonstrate quantitatively how the microstructure has helped the catalysis, however, due to the high specific surface area exhibiting more active sites and the fact that the •OH radicals are produced at the catalyst/water interface under UV light illumination, the density of •OH radicals becomes more and more bigger in the direction from the center of nano-tubes to the inner surface of nano-tubes. Meantime, the confinement both in the latitudinal and radial direction within the arrays force the RhB molecules to flow through the nano-tubes leading to more opportunities to access the produced reactive •OH radicals which can decompose RhB

into different species (Table 2) besides CO₂. As a result, the nanotubular arrays present unique capabilities.

Renewable catalytic activity of the PEI/PSS/(PAH/PSS)₃(PAH/PW₁₂)₈ nano-tubular arrays

Under the obtained optimal condition, renewal and reuse of the nano-tubular arrays was tested. In the experiment, 5 overlapped PW₁₂-AAOs and 5 overlapped PW₁₂-PCs were used as catalyst for filtering RhB solution, respectively. It was observed that catalytic activity of the nano-tubular arrays in both AAO and PC faded after successive reuse (Fig. S9). This could be due to the loss of the POMs on the inner surface of the nano-tubes and meantime indicates that leached POMs into the solution can not catalysis as effective as those with the nano-tubular arrays because of the absence of confinement both in the latitudinal and radial direction. Importantly, the catalytic activity of the POMs nano-tubular arrays can be fully renewed by simple immersion in a H₃PW₁₂O₄₀-containing mother solution (Fig.11) and can be reused as efficiently as fresh catalysts. Obviously, this is very important in view of practical application.

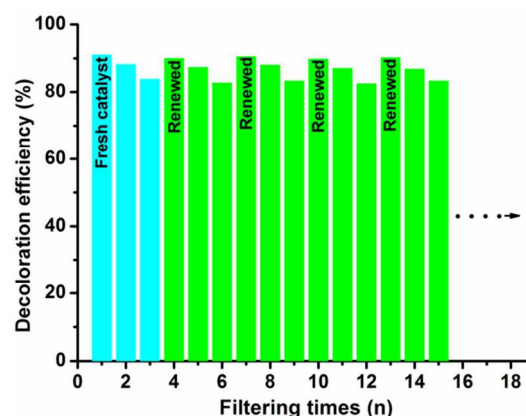


Fig.11. Catalytic activity of fresh catalyst (5 overlapped PW₁₂-PCs) (cyan column) and the renewed catalysts (green column). Each renewal process was conducted after the catalyst had been used to photo-degrade fresh RhB solution for three times.

Conclusion

In summary, we successfully prepared PEI/PSS/(PAH/PSS)₃(PAH/PW₁₂O₄₀³⁻)₈ nano-tubular arrays in porous templates AAO and PC by LBL method as a prototype, which not only allowed the precise structural design (controllable wall thickness and aperture) and control of the geometrical features (linear growth and smooth surface) but also solved the template pore blocking problem by combination of reduced pressure filtration process and neutral washing steps. The fabricated POM nano-tubular arrays exhibited excellent effect on photo-degradation of RhB under mild condition and the catalytic activity of the POMs nano-tubular arrays can be fully renewed by simple immersion in a H₃PW₁₂O₄₀-containing mother solution when catalytic reactivity gets faded. Effort to get POMs anchored on the inner tube surface by relatively stronger covalent bonds are also under taken to avoid even less leaching of POMs in the economical and environmental view. Given the large number of polyoxometalates of various structures and properties reported in the literature, this work

may provide new concepts for catalyst designing and regeneration based on polyoxometalates with nano-confinement effect, array effect and coupling effect, which show extensive potential/practical application in designing reactors with specific sizes for specific reaction systems.

Acknowledgements

The financial support of the Natural Science Foundation of China, PCSIRT(No. IRT1205), the Fundamental Research Funds for the Central Universities (YS1406) and Beijing Engineering Center for Hierarchical Catalysts is greatly acknowledged. Prof. Xue Duan of Beijing University of Chemical Technology is greatly acknowledged for his kind support.

Notes and references

^a State Key Laboratory of Chemical Resource Engineering, Beijing University of Chemical Technology, Beijing 100029, China; ^b College of Materials Science and Engineering, Beijing University of Chemical Technology, Beijing 100029, China

Electronic Supplementary Information (ESI) available: Figures s1-s9, Table S1. DOI: 10.1039/b000000x/

*Corresponding author. Tel.: +86-10-64414640; e-mail: zhouys@mail.buct.edu.cn; ljzhang@mail.buct.edu.cn

- C. L. Hill, A themed issue on polyoxometalate chemistry in *Chem. Rev.*, 1998, **98**, 1-387.
- P. Kögerler, B. Tsukerblat and A. Müller, *Dalton Trans*, 2010, **39**, 21-36.
- L. Cronin and A. Müller, A themed issue on polyoxometalate chemistry in *Chem. Soc. Rev.*, 2012, **41**, 9799-10106; D. Long and L. Cronin, A themed issue entitled Polyoxometalate Cluster Science in *Chem. Soc. Rev.*, 2012, **41**, 7325-7633.
- M. Misono and N. Nojiri, *Appl. Catal.*, 1990, **64**, 1-30.
- C. L. Hill and C. M. Prosser-McCartha, *Coord. Chem. Rev.*, 1995, **143**, 407-455.
- T. Okada, K. Miyamoto, T. Sakai and S. Mishima, *ACS Catal.*, 2014, **4**(1), 73-78.
- C. W. Hu, M. Hashimoto, T. Okuharan and M. Misono, *J. Catal.*, 1993, **143**, 437-438.
- A. Hiskia, A. Mylonas and E. Papaconstantinou, *Chem. Soc. Rev.*, 2001, **30**, 62-69.
- M. Misono, *Chem. Commun.*, 2001, **13**, 1141-1152.
- M. A. Fox, R. Cardona and E. Gaillard, *J. Am. Chem. Soc.*, 1987, **109**, 6347-6354.
- C. L. Hill and D. A. Bouchard, *J. Am. Chem. Soc.*, 1985, **107**, 5148-5157.
- R. Noyori, M. Aoki and K. Sato, *Chem. Commun.*, 2003, **16**, 1977-1986.
- M. T. Pope, *Heteropoly and Isopoly-Oxometalates*, Springer-Verlag, Berlin, 1983.
- D. A. Friesen, L. Morello, J. V. Headley and C. H. Langford, *J. Photochem. Photobiol. A: Chem.*, 2000, **133**, 213-220.
- C. C. Chen, Q. Wang, P. X. Lei, W. J. Song, W. H. Ma and J. C. Zhao, *Environ. Sci. Technol.*, 2006, **40**, 3965-3970.
- T. Ito, K. Inumaru and M. Misono, *J. Phys. Chem. B*, 1997, **101**, 9958-9963.
- J. Haber, K. Pamin, L. Matachowski, B. Napruszewska and J. Poltowicz, *J. Catal.*, 2002, **207**, 296-306.
- C. Ramesh Kumar, N. Rambabu, K. C. Maheria, A. K. Dalai and N. Lingaiah, *Appl. Catal., A*, 2014, **485**, 74-83.
- A. Maldotti, A. Molinari and F. Bigi, *J. Catal.*, 2008, **253**, 312-317.
- J. D. Torres, E. A. Faria, J. R. DeSouza and A. G. S. Prado, *J. Photochem. Photobiol. A*, 2006, **182**, 202-206.
- C. J. Yang, L. H. Tian, L. Q. Ye, T. Y. Peng, K. J. Deng and L. Zan, *J. Appl. Polym. Sci.*, 2011, **120**, 2048-2053.
- S. Iijima, *Nature*, 1991, **354**, 56-58.
- Y. N. Xia, P. D. Pang, Y. G. Sun, Y. Y. Wu, B. Mayers, B. Gates, Y. D. Yin, F. Kim and H. Q. Yan, *Adv. Mater.*, 2003, **15**, 353-389.
- C. Marchena, R. A. Frenzel, S. Gomez, L. B. Pierella and L. S. Pizzio, *Appl. Catal. B*, 2013, **130-131**, 187-196.
- S. Y. Gao, R. Cao, J. Lv, G. L. Li, Y. F. Li and H. X. Yang, *J. Mater. Chem.*, 2009, **19**, 4157-4163.
- Y. You, S. Y. Gao, Z. Yang, M. N. Cao and R. Cao, *J. Colloid Interface Sci.*, 2012, **365**, 198-203.
- C. C. Chen, Q. Wang, P. X. Lei, W. J. Song, W. H. Ma and J. C. Zhao, *Environ. Sci. Technol.*, 2006, **40**, 3965-3970.
- P. X. Lei, C. C. Chen, J. Yang, W. H. Ma, J. C. Zhao and L. Zang, *Environ. Sci. Technol.*, 2005, **39**, 8466-8474.
- J. H. Li, W. L. Kang, X. Yang, X. D. Yu, L. L. Xu, Y. H. Guo, H. B. Fang and S. D. Zhang, *Desalination*, 2010, **255**, 107-116.
- S. Kim, J. Yeo and W. Choi, *Appl. Catal. B: Environ.*, 2008, **84**, 148-155.
- N. Lu, Y. H. Zhao, H. B. Liu, Y. H. Guo, X. Yuan, H. Xu, H. F. Peng and H. W. Qin, *J. Hazard. Mater.*, 2011, **199-200**, 1-8; Q. Wang, M. Zhang, C. Chen, W. Ma and J. Zhao, *Angew. Chem. Int. Ed.*, 2010, **49**, 7976-7979.
- M. Huang, X. Han, C. Hung, J. Lin, P. Wu, J. Wu and S. Liu, *J. Catal.*, 2014, **320**, 42-51.
- E. Androulaki, A. Hiskia, D. Dimotikali, C. Minero, P. Calza, E. Pelizzetti and E. Papaconstantinou, *Environ. Sci. Technol.*, 2000, **34**, 2024-2028; J. Yu, G. Dai, B. Cheng, *J. Phys. Chem. C.*, 2010, **114**, 19378-19385.34 D. M. Sullivan and M. L. Bruening, *Chem. Mater.*, 2003, **15**, 281-287.
- A. L. Souza, F. G. Tremiliosi, L. T. Kubota, R. K. Mendes, A. M. Botelho do Rego, O. N., Jr. Oliveira, C. Henry de Villeneuve, J. N. Chazalviel, P. Allongue, F. Ozanam and U. P. Rodrigues Filho, *RSC Advances*, 2014, **4**(56), 29612-29621; N. Gu, D. Wei, L. Niu and A. Ivaska, *Electrochimica Acta*, 2006, **51**(27), 6038-6044.
- Z. X. Sun, L. Xu, W. H. Guo, B. B. Xu, S. P. Liu and F. Y. Li, *J. Phys. Chem. C*, 2010, **114**, 5211-5216.
- Y. J. Wei, Z. M. Kang and C. G. Liu, *Spectro. Spectral Anal.*, 2004, **24**, 1659-1662.
- C. C. Chen, W. Zhao, P. X. Lei, J. C. Zhao and N. Serpone, *Chem. Eur. J.*, 2004, **10**, 1956-1965.
- A. Mylonas and E. Papaconstantinou, *J. Photochem. Photobiol. A: Chem.*, 1996, **94**, 77-82; A. Hiskia and E. Papaconstantinou, *Inorg. Chem.*, 1992, **31**, 163-167.